RSC Advances

PAPER

Cite this: *RSC Adv.*, 2015, **5**, 10072

Effect of alkyl-chain branching position on nanoscale morphology and performance of all-polymer solar cells†

Fangbin Liu,[ab] Hui Li,[ab] Chunling Gu*[a] and Hongbing Fu*[a]

Manipulating the alkyl-chain branching position afforded two naphthalene diimide-based polymers (**C1** and **C3**). The optoelectronic properties, including the absorption spectra and electronic energy levels, conformations and photovoltaic properties of the two polymers, were fully studied and compared. The effect of alkyl-chain branching position on their optoelectronic properties and crystallinity was investigated in detail. Moving the branching position away from the backbone resulted in superior crystallinity of **C3**. All-polymer solar cells (all-PSCs) based on **C1** or **C3** as the acceptor and polymer PBDTTT-C-T as the donor were fabricated and optimized. The power conversion efficiencies (PCEs) of the optimized all-PSCs based on **C1** and **C3** reached 1.68% and 1.92%, respectively. The improved photovoltaic performance may be due to the clear nanoscale morphology of **C3**-based blend film. The blend film exhibits favorable phase separation and well-ordered structure of polymer **C3**. This substantially increased the electron mobility (up to 1.0×10^{-4} cm^2 V^{-1} s^{-1}), which contributes to balancing the charge transport in **C3**-based blend film. This is the first report on the realization of favorable phase separation and high electron mobility through improvement of acceptor crystallinity in all-PSCs.

Received 28th October 2014
Accepted 18th December 2014

DOI: 10.1039/c4ra13351j

www.rsc.org/advances

Introduction

All-polymer solar cells (all-PSCs) have received much attention in recent years, as they provide a facile and low-cost way to utilize solar energy.[1–4] π-Conjugated polymers as acceptor materials in all-PSCs have potential advantages. In comparison with fullerene derivatives, π-conjugated polymers can be easily chemically synthesized and modified. They have broad absorption spectra and high absorption coefficients, and possess fine-tuned energy levels to match the donor polymer.[4–7] However, all-PSCs are still being advanced slowly with low power conversation efficiency (PCE) with, for example, performance based on backbones of naphthalene diimide (5.7%),[8] perylene diimide (4.4%),[9] fluorene (2.0%),[7,10] and carbazol (3.68%).[11] The relatively low efficiency has been considered to be due to the unfavorable morphology of bulk heterojunction (BHJ) blend films such as weak phase separation[12] and reduced ordering of polymer chains.[13] A significant challenge for π-conjugated polymers as alternative acceptors to replace fullerene derivatives is to improve the phase separation and charge transport ability.[14] Therefore, acceptor polymers with high crystallinity or aggregation ability are highly desired, similar to fullerene derivatives,[14–16] to realize high phase separation and electron mobility in all-PSCs.

From the viewpoint of molecular design, polymer crystallinity is significantly related to the planarization of polymer backbones which can be achieved by modifying the molecular structure of π-functional backbones and the pattern of alkyl side chains.[17–23] The latter has been widely accepted to impact on the morphology (crystallization, π-stacking and packing orientation), charge transport and photovoltaic performance of devices.[24–27] Takimiya's group found that different linear and branched alkyl side chains altered the polymer orientation, thus affecting the PCEs of devices.[28] It should be mentioned that previous investigations were limited to the study of donor polymer alkyl chains, including alkyl chain length and branching point;[29–35] however, the effect of alkyl-chain branching position in acceptor polymers on the performance has not been reported for all-PSCs. Detail studies on the critical role of alkyl chains in photovoltaic performance of all-PSCs are thus highly desired. Furthermore, the manipulation of alkyl-chain branching position should be an important strategy to design polymers with good crystallinity and achieve high performance as acceptors in all-PSCs.

---

[a] *Beijing National Laboratory for Molecular Sciences (BNLMS), Institute of Chemistry, Chinese Academy of Sciences, 100190, Beijing, P. R. China. E-mail: hongbing.fu@iccas.ac.cn; chunlgu@iccas.ac.cn*

[b] *University Chinese Academy of Sciences, Beijing 100049, P. R. China*

† Electronic supplementary information (ESI) available: Details of for the measurement of cyclic voltammogram and charge mobilities, TGA images and AFM images. See DOI: 10.1039/c4ra13351j

Due to the highly electron-deficient character of naphthalene diimide (NDI),[36,37] NDI-based derivatives possess deep low unoccupied molecular orbital (LUMO) energy levels, which make them good electron transporting semiconductors and suitable acceptor materials for PSCs. As a result, NDI-based copolymers have attracted much attention in the fields of PSCs and organic field effect transistors (OFETs).[4,37–43] In previous studies, a typical NDI-bithiophene copolymer (PNDI-TT) with good aggregation ability was initially proved to exhibit low PCEs of 0.2–1.4% in all-PSCs.[42–46] Very recently, Ito's group reported high PCE of above 4% based on the same polymer as acceptor *via* significantly enhancing charge-carrier generation and collection efficiencies.[8,47] At the same time, Liu *et al.* reported that the introduction of vinyl groups into the copolymer backbone of PNDI-TT could improve the charge mobility of neat film in OFETs.[38] It is proved that vinyl groups can extend the polymer coplanarity as well as the intermolecular π–π stacking, which would enhance the polymer crystallinity with negligible influence on the low-lying LUMO energy level. Herein, we focus on the manipulation of the branching position of alkyl chains to improve polymer crystallinity, which would be beneficial to increase the PCE *via* favorable phase separation in all-PSCs.

In this study, we successfully designed and synthesized polymers **C1** and **C3**, where C*m* refers to the number of linear carbon atoms between the alkyl-chain branching position and the alkylated nitrogen (Fig. 1). A systematic study of their optical, electronic, and conformation properties, and the characteristics of all-PSCs based on these polymers are described. For comparision, a detailed structural analysis of these polymers was performed using grazing incidence X-ray diffraction (GIXD) and transmission electron microscopy (TEM) to elucidate the effect of the branching position on polymer crystallinity and morphology of blend films. It was found that the morphologies of all-polymer BHJ films strongly depend on the alkyl-chain branching position. Better device performance was obtained from polymer **C3** with superior crystallinity where a PCE of 1.92% was obtained under AM 1.5G illumination with 3% 1,8-diiodooctane (DIO) as processing additive. The improved performance arises from the clear nanoscale morphology with favorable phase separation and well-ordered domains. Our results provide an example for rational design criteria of polymer acceptors to realize nanoscale phase separation morphology and high electron mobility.

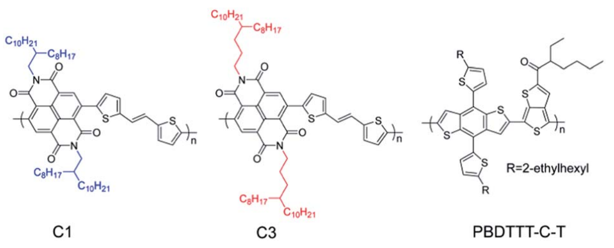

Fig. 1 Chemical structures of polymers **C1**, **C3** and donor polymer PBDTTT-C-T.

Experimental section

Materials

The polymers PBDTTT-C-T were purchased from Solarmer Materials Inc. and used as received. The number-average molecular weight (M_n) and polydispersity index (PDI; given by M_w/M_n, where M_w is the weight-average molecular weight) provided on the Certificate of Analysis, were 54.9 kg mol^{-1} and 1.9, respectively. 2-(Tributylstannyl)thiophene, NBS, and *trans*-1,2-bis(tributylstannyl)ethene were purchased from Sigma-Aldrich. Compounds 2-octyldodecan-1-amine (**2a**) and 4-octyltetradecan-1-amine (**2b**) were purchased from LYN (Beijing) Technology Co. Ltd. Compound 2,6-dibromo-1,4,5,8-naphthalene tetracarboxylic dianhydride (**1**) was synthesized according to the literature.[36,37] Toluene was dried over Na/benzophenoneketyl and freshly distilled before use. The other reagents and solvents used in this work were commercially purchased and used without further purification. All air- and water-sensitive reactions were performed under nitrogen atmosphere. The detailed synthetic processes of the other compounds are as follows.

Synthetic procedures

***N*,*N*′-Bis(4-octyltetradecyl)-2,6-dibromo-1,4,5,8-naphthalene diimide (3b).** A mixture of **1** (2.12 g, 5.0 mmol), 4-octyltetradecylamine (4.07 g, 12.5 mmol), and acetic acid (100 mL) was stirred at 110 °C for 12 h. After cooling to room temperature, most of the solvent was removed under vacuum, and the residue was purified by column chromatography on silica gel with a mixture of ethyl acetate/petroleum ether (1 : 60, v/v) as eluent, affording a slightly yellow solid as the product (1.30 g, 1.25 mmol, yield 25%). ^{1}H NMR (CDCl$_3$, 400 MHz) δ: 8.98 (s, 2H), 4.16 (d, J = 7.6 Hz, 4H), 1.70 (m, 4H), 1.32–1.41 (m, 6H), 1.15–1.35 (m, 64H), 0.85–0.89 (m, 12H); ^{13}C NMR (CDCl$_3$, 400 MHz) δ: 160.60, 138.97, 128.27, 127.60, 125.28, 124.01, 77.45, 77.03, 76.61, 41.49, 37.22, 33.54, 31.93, 30.96, 30.10, 29.71, 29.66, 29.37, 26.67, 25.15, 22.69, 14.13; MS-TOF [M]$^+$: 1040.5 (*m*/*z*).

***N*,*N*′-Bis(2-octyldodecyl)-2,6-dibromo-1,4,5,8-naphthalene diimide (3a).** A mixture of **1** (1.92 g, 4.5 mmol), 2-octyldodecan-1-amine (3.35 g, 11.25 mmol), and acetic acid (90 mL) was stirred at 110 °C for 12 h. A slightly yellow solid (1.37 g, 1.40 mmol, yield 31%) was obtained using the same processing method as for compound **3a.** ^{1}H NMR (CDCl$_3$, 400 MHz) δ: 8.95 (s, 2H), 4.12 (d, J = 7.5 Hz, 4H), 1.97 (m, 2H), 1.20–1.40 (m, 64H), 0.84–0.89 (m, 12H); MS-TOF [M]$^+$: 984.5 (*m*/*z*).

***N*,*N*′-Bis(4-octyltetradecyl)-2,6-bis([2,2′]-bithiophenyl-5-yl)-1,4,5,8-naphthalene diimide (4b).** Compound **3b** (1.04 g, 1.0 mmol), 5-tributylstannyl-2,2′-bithiophene (0.94 g, 2.5 mmol), Pd(PPh$_3$)$_2$Cl$_2$ (98 mg, 0.1 mmol) and 20 mL of anhydrous toluene were added to a flask under argon. The mixture was refluxed for 16 h and then cooled down to room temperature. After quenching with CaF$_2$·12H$_2$O, the solvent was removed under vacuum and the product was purified by column flash chromatography using an ethyl acetate/petroleum ether solvent mixture (10 : 1). The pure product was obtained as a red solid (943 mg, 0.9 mmol, yield 90%). ^{1}H NMR (CDCl$_3$, 400 MHz) δ:

8.77 (s, 2H), 7.78 (d, 4H), 7.31 (d, 2H), 7.21 (d, 2H), 4.10 (d, $J = 7.6$ Hz, 4H), 1.70 (m, 4H), 1.32–1.41 (m, 6H), 1.15–1.35 (m, 64H), 0.85–0.89 (m, 12H); ^{13}C NMR ($CDCl_3$, 400 MHz) δ: 162.13, 161.96, 140.73, 140.28, 136.62, 128.85, 127.94, 127.46, 127.39, 125.43, 123.47, 77.34, 77.03, 76.71, 41.48, 37.31, 33.58, 31.92, 31.01, 30.11, 29.69, 29.65, 29.35, 26.68, 25.34, 22.68, 14.10; MS-TOF $[M]^+$: 1046.8 (*m*/*z*).

***N*,*N*′-Bis(2-octyldodecyl)-2,6-bis([2,2′]-bithiophenyl-5-yl)-1,4,5,8-naphthalene diimide (4a).** Compound **3a** (1.37 g, 1.4 mmol), 5-tributylstannyl-2,2′-bithiophene (1.32 g, 3.5 mmol), $Pd(PPh_3)_2Cl_2$ (137.2 mg, 0.14 mmol) and 20 mL of anhydrous toluene were added to a flask under argon. A red solid (1.24 g, 1.25 mmol, yield 89%) was obtained with the same processing method as for compound **4a.** ^{1}H NMR ($CDCl_3$, 400 MHz) δ: 8.74 (s, 2H), 7.54 (d, $J = 5.1$ Hz, 2H), 7.28 (d, $J = 3.6$ Hz, 2H), 7.18 (m, 2H), 4.05 (d, $J = 7.2$ Hz, 4H), 1.93 (m, 2H), 1.23 (m, 64H), 0.86 (m, 12H); MS-TOF $[M]^+$: 990.8 (*m*/*z*).

***N*,*N*′-Bis(4-octyltetradecyl)-2,6-bis(5-bromothiophenyl-5-yl)-1,4,5,8-naphthalene diimide (5b).** Compound **4b** (524 mg, 0.5 mmol) was dissolved in 25 mL of chloroform. NBS (214 mg, 1.2 mmol) was added to the reaction mixtures. After stirring in the dark for two days, the product was extracted with dichloromethane and washed with brine, and the organic layer was evaporated. The red solid was purified by column chromatography using an ethyl acetate/petroleum ether (1 : 50) solvent mixture to give the final product as a red solid (493 mg, 0.41 mmol, yield 82%). ^{1}H NMR ($CDCl_3$, 400 MHz) δ: 8.72 (s, 2H), 7.15 (d, $J = 3.9$ Hz, 2H), 7.08 (d, $J = 3.9$ Hz, 2H), 4.10 (d, $J = 5.6$ Hz, 4H), 1.55 (m, 4H), 1.24 (m, 64H), 0.85–0.87 (m, 12H); ^{13}C NMR ($CDCl_3$, 400 MHz) δ: 161.89, 142.05, 139.11, 136.44, 130.18, 128.85, 127.50, 125.63, 123.21, 115.50, 77.47, 77.05, 76.62, 41.57, 37.27, 33.55, 31.94, 30.99, 30.12, 29.71, 29.67, 29.37, 26.67, 25.32, 22.70, 14.14; MS-TOF $[M]^+$: 1205.4 (*m*/*z*).

***N*,*N*′-Bis(2-octyldodecyl)-2,6-bis(5-bromothiophenyl-5-yl)-1,4,5,8-naphthalene diimide (5a).** Compound **4a** (1.09 g, 1.1 mmol) was dissolved in 25 mL of chloroform. NBS (235.0 mg, 1.32 mmol) was added to the reaction mixture. A red solid (1.08 g, 0.935 mmol, yield 85%) was obtained with the same processing method as for compound **5a.** ^{1}H NMR ($CDCl_3$, 400 MHz) δ: 8.77 (s, 2H), 7.44 (d, $J = 3.9$ Hz, 2H), 7.08 (d, $J = 3.9$ Hz, 2H), 4.07 (d, $J = 7.2$ Hz, 4H), 1.94 (m, 2H), 1.24 (m, 64H), 0.85 (m, 12H); MS-TOF $[M]^+$: 1148.4 (*m*/*z*).

Preparation of poly[*N*,*N*′-bis(4-octyltetradecyl)-2,6-bis([2,2′]-bithiophenyl-5-yl)-1,4,5,8-naphthalene diimide-5′,5‴-diyl]-*alt*-*trans*-ethylene (C3). Compound **5b** (120.5 mg, 0.1 mmol), *trans*-1,2-bis(tributylstannyl)ethane (6.6 mg, 0.1 mol), $Pd_2(dba)_3$ (9.2 mg, 0.01 mol), P(*o*-tol)$_3$ (12.2 mg, 0.04 mol) and 3 mL of toluene were added to a Schlenk tube. The tube was charged with nitrogen through a freeze–pump–thaw cycle for three times. The mixture was stirred for 48 h at 110 °C. The mixture was cooled to room temperature and precipitated into methanol (100 mL). The precipitate was filtered through a nylon filter, purified *via* Soxhlet extraction for 12 h with methanol, acetone, hexane, chloroform, and chlorobenzene, and finally collected with dichlorobenzene. The dichlorobenzene solution was then concentrated by evaporation, precipitated into methanol (100 mL), and filtered off to afford a dark blue solid (77.5 mg, yield 61%).

Poly[*N*,*N*′-bis(2-octyldodecyl)-2,6-bis(thiophenyl-5-yl)-1,4,5,8-naphthalene diimide-2,2′-diyl]-*alt*-*trans*-ethylene (C1). Compound **5a** (229.8 mg, 0.20 mmol), *trans*-1,2-bis(tributylstannyl)ethane (13.2 mg, 0.20 mol), $Pd_2(dba)_3$ (18.2 mg, 0.02 mol), P(*o*-tol)$_3$ (24.2 mg, 0.08 mol) and 5 mL of toluene were added to a Schlenk tube. The same processing method as for polymer **C3** was used during polymerization and purification. After Soxhlet extraction, the product was finally collected with chlorobenzene. Dark blue solid, 147.4 mg, yield 58%.

Measurements and characterization

^{1}H NMR spectra and ^{13}C NMR spectra were measured with a Bruker DMX-400 spectrometer in $CDCl_3$ (^{1}H, δ: 7.26 ppm; ^{13}C, δ: 77 ppm) with tetramethylsilane (TMS) as the internal standard. Gel permeation chromatography (GPC) was performed with a Polymer Laboratories PL 220 at 150 °C using 1,2,4-tricholorobenzene as eluent. The obtained molecular weight was calibrated with polystyrene standards. Thermogravimetric analysis (TGA) was done using a TA Instruments NETZSCH STA 409 PC/PG analyzer operated at a heating rate of 10 °C min^{-1} and under a nitrogen atmosphere. UV-visible (UV-vis) absorption spectra were obtained with a Shimidazu UV-3600 UV-vis-NIR spectrophotometer. The structural properties of polymers were determined by GIXD measurements on thin films produced by dropping 1,2-dichlorobenzene (DCB) solutions of polymer onto Si substrate. The thickness of the functional layers was measured using a KLA-T encore P-6 profilometer (Tencor). The morphology and surface roughness of the layers were determined by atomic-force microscopy (AFM; Digital Instruments Nano Scope III). TEM images were obtained with a JEM-2100 transmission electron microscope operated at an acceleration voltage of 200 kV. The sample used in AFM and TEM measurement was from the naked active layer in devices. Cyclic voltammetry measurements were performed using a Zahner IM6e electrochemical workstation with a three-electrode system in a solution of 0.1 M Bu_4NPF_6 in anhydrous acetonitrile at a scan rate of 50 mV s^{-1}.

PSC device fabrication and measurement

The PSC devices were fabricated with a structure of ITO/PEDOT:PSS/active layer/Ca/Al, where the active layer was composed of **C1** or **C3** as acceptor and polymer PBDTTT-C-T as donor. Patterned ITO-glass substrates were used as the anode in PSCs. ITO substrates were firstly pre-cleaned sequentially by sonicating in a detergent bath, deionized water, acetone, and isopropanol each for 20 min, and then dried in an oven for 30 min, and lastly cleaned in a UV/ozone cleaner for 60 min. A thin layer of poly(3,4-ethylenedioxythiophene) (PEDOT):poly(styrene sulfonate) (PSS) was spin-cast onto the ITO surface. After being baked at 150 °C for 20 min in ambient air, the substrates were transferred into a nitrogen-filled glove box (<0.1 ppm O_2 and H_2O). **C1** or **C3** was blended with polymer PBDTTT-C-T and dissolved in DCB. The active layers were then spin-cast from the blend solutions (20 mg mL^{-1}, polymer weight concentration) with various rotational speeds on the ITO/PEDOT:PSS substrates. A small amount of DIO was used as an additive to improve the photovoltaic performance of the devices if necessary. Beside this, no further treatment to the blend film was performed before the deposition of the metal electrode. Finally, a Ca/Al metal top electrode was deposited under vacuum onto the active layer at a pressure of *ca.* 5×10^{-5} Pa. The active area of the device was *ca.* 6.0 mm^2. The current density–voltage (J–V) characteristics were measured with a computer-controlled Keithley 2400 Source Measure Unit. A xenon lamp coupled with an AM 1.5 solar spectrum filter was used as the light source, and the optical power was 100 mW cm^{-2}. The EQE measurements of the encapsulated devices were performed in air (PV Measurements Inc., model QEX7). The hole and electron mobilities were calculated by fitting the dark J–V curves for the hole-only and electron-only devices to the space-charge-limited-current (SCLC) model at low voltages.

Results and discussion

Synthesis and characterization

The synthetic routes of the monomers and corresponding polymers are outlined in Scheme 1. Polymers **C1** and **C3** were synthesized by Stille coupling reaction between the dibromide monomers (**3a** and **3b**) and the *trans*-1,2-bis(tributylstannyl) ethene using $Pd_2(dba)_3$ as the catalyst. The obtained polymers were precipitated in methanol and then purified by Soxhlet extraction to remove oligomers and other impurities. The number-average molecular weights (M_n) and polydispersity indices (PDIs) were 23.0 kDa, 3.5 and 74.5 kDa, 2.7 for **C1** and **C3** respectively, evaluated by high-temperature GPC at 150 °C using 1,2,4-tricholorobenzene as eluent. The two polymers had molecular weights of more than 20 kg mol^{-1}, which is considered to be quite high for low bandgap polymers.[48–50] In our work, the effect of molecular weight of the two polymers is a negligible factor according to the similar performance of BHJ solar cells in unoptimized devices. The TGA measurements showed that the onset temperatures (T_d) of **C1** and **C3** with 5% weight loss are over 430 °C.

Optoelectronic and electrochemical properties

The optical properties of **C1** and **C3** were measured in toluene solution and as thin films (Fig. 2), and the detailed absorption data are collected in Table 1. Those polymers show similar broad absorption spectral features across the entire UV-vis region in toluene solution. As for polymers comprised of donor and acceptor units, the absorption spectrum is characterized by two spectral features, a high-energy peak and a broad low-energy band.[41,51] The high-energy peak located at approximately 400 nm can be attributed to the π–π* transition in the polymeric backbone. The low-energy band with major absorption peaks at 678 nm for **C1** and 684 nm for **C3** is ascribed to the charge-transfer transition between electron-donating ethylene units and electron-deficient NDI units. In the solid state, the main absorption bands become broader, and red shifts occur of the maximum absorption peaks at 716 nm and 726 nm by 38 nm and 42 nm, relative to those in solution, for **C1** and **C3** respectively. These large red shifts from solution to thin film are indicative of a planarization of the conjugated backbone and strong interchain π–π stacking in the solid state. Notably, the absorption spectrum of **C3** film exhibits a sharp shoulder peak at 805 nm while that of **C1** film does not, which may originate from more efficient stacking in polymer **C3**. The absorption edges (λ_{onset}) of the two polymer films are 890 nm for **C1** and 895 nm for **C3**, from which the optical band gaps (E_g^{opt}) of the polymers can be calculated according to $E_g^{\text{opt}} = 1240/\lambda_{\text{onset}}$. E_g^{opt} values of **C1** and **C3** are 1.40 and 1.38 eV, respectively.

Cyclic voltammetry measurements were carried out to evaluate the electrochemical properties and estimate the HOMO/LUMO energy levels of the two polymers (Fig. S1†). Our results are similar to the data of previous work by Liu *et al.*[38] As we expected, the changes of alkyl-chain branching position have a negligible effect on polymer energy levels.[28–31,35] As listed in Table 1 and shown in Fig. 2b, the HOMO/LUMO energy values of **C1** and **C3** are −5.61/−3.93 eV and −5.61/−3.94 eV. The

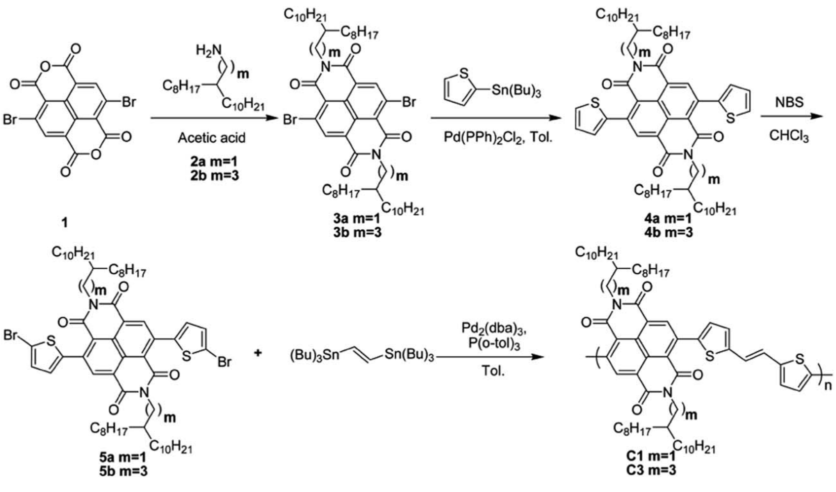

Scheme 1 Synthesis routes of the monomers and conjugated polymers **C1** and **C3**.

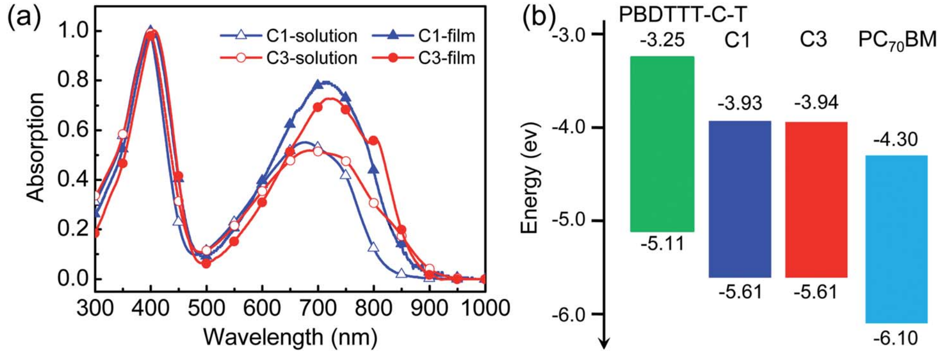

Fig. 2 (a) Normalized UV-vis absorption spectra of **C1** and **C3** in toluene solution and as thin films. (b) HOMO and LUMO energy levels of the polymers and $PC_{70}BM$.

energy levels of the polymers are well matched with those of polymer PBDTTT-C-T[52] and the LUMO energies are significantly higher-lying than that of $PC_{70}BM$ (Fig. 2b); thus, a large V_{oc} could be expected to occur in the corresponding devices.

GIXD characterization

To study the effect of alkyl-chain branching position of the polymers on the packing orientation and crystallinity of films, GIXD was performed. As seen in Fig. 3 and S3,† an edge-on orientation was found for both thin films, with evident (100) diffraction peaks in the out-of-plane direction. The d_{100} spacings corresponding to out-of-plane space distance between polymer backbones are 23.2 Å for **C1** and 26.0 Å for **C3**. This kind of spacing related to the side-chain length is much shorter than that of fully extended alkyl chains, indicating that side chains of polymer in adjacent layers were closely interdigitated in lamellar structures.[23,53] Noticeably, an obvious (200) diffraction at 6.80° and (001) diffraction halos of alkyl chains[38] at 5.68° for polymer **C3** demonstrate that polymer **C3** possesses superior crystallinity ability compared with polymer **C1**. Therefore, moving the branching position away from the conjugated backbone may reduce the steric effect of bulk octyldodecyl chain and promote the ordering of lamellar structure of the polymer.

Photovoltaic properties

All-PSCs were fabricated by employing **C1** or **C3** as acceptor material and PBDTTT-C-T as donor material (Fig. 1), with a conventional device structure of ITO/PEDOT:PSS/PBDTTT-C-T : polymer/Ca/Al. The best weight ratio of PBDTTT-C-T : polymer was 1 : 1 (w/w). Fig. 4a displays the current density–voltage (*J*–*V*) curves of the devices under illumination of AM 1.5G simulated white light with an intensity of 100 mW cm^{-2}. The V_{oc}, short circuit current density (J_{sc}), fill factor (FF) and PCE of the devices are shown in Table 2 and Fig. 4. The other device data are summarized in the ESI.†

Devices fabricated from a blend of **C1** with PBDTTT-C-T gave a J_{sc} of 3.64 mA cm^{-2}, a V_{oc} of 0.81 V and a FF of 0.49, corresponding to a PCE of 1.21%. When the linear chain increased to three carbon atoms in **C3**, devices showed a slight improvement in the photovoltaic performance, with a PCE of 1.27%, which indirectly demonstrated that molecular weight has little effect on photovoltaic performance. In order to further improve the PCE, DIO was used as a processing additive.[54–56] When 1% DIO was added, the photovoltaic performance based on **C1** was further improved to 1.68%, with a J_{sc} of 3.64 mA cm^{-2}; the highest PCE of 1.92% was achieved by adding 3% DIO to PBDTTT-C-T/**C3** devices, with a highest J_{sc} of 4.70 mA cm^{-2}. However, further increasing the ratio of DIO resulted in a gradual decrease in photovoltaic performance for both **C1** and **C3** (Table S1†). Charge mobilities of the optimal blend films based on polymers **C1** and **C3** were measured using the charge-only SCLC method as shown in Fig. S4.† Hole and electron mobilities of PBDTTT-C-T : polymer BHJ devices were estimated to be, respectively, 1.3×10^{-4} cm^2 V^{-1} s^{-1} and 6.6×10^{-5} cm^2 V^{-1} s^{-1} for **C1**, and 1.8×10^{-4} cm^2 V^{-1} s^{-1} and 1.0×10^{-4} cm^2 V^{-1} s^{-1} for **C3**. It is noteworthy that electron mobility in **C3**-based active layers is much higher than that in layers based on **C1**, and equal to the hole mobility value. The balanced hole and electron motilities in the **C3**-based blend film can largely explain the high performance of the BHJ solar cells.[2] On account

Table 1 Basic properties of polymers (molecular weights, thermostability, optical and electrochemical properties)

Cn	M_n[a] (kDa)	M_w[a] (kDa)	PDI[a]	T_d[b] (°C)	λ_{max}[c] (nm)	λ_{max}[d] (nm)	λ_{onset}[d] (nm)	E_g^{opte} (eV)	E_{HOMO} (eV)	E_{LUMO} (eV)
C1	23.0	79.9	3.5	433	395, 678	403, 716	890	1.40	−5.61	−3.93
C3	74.5	197.8	2.7	445	396, 684	405, 726, 805	895	1.38	−5.61	−3.94

[a] Determined by GPC in trichlorobenzene at 150 °C using polystyrene standards. [b] Decomposition temperature, determined by TGA in nitrogen at a heating rate of 10 °C min^{-1}, based on 5% weight loss. [c] Measured in dilute toluene solution. [d] Spin-cast from 4 mg mL^{-1} dichlorobenzene solution. [e] Optical band gap calculated from the onset of film absorption.

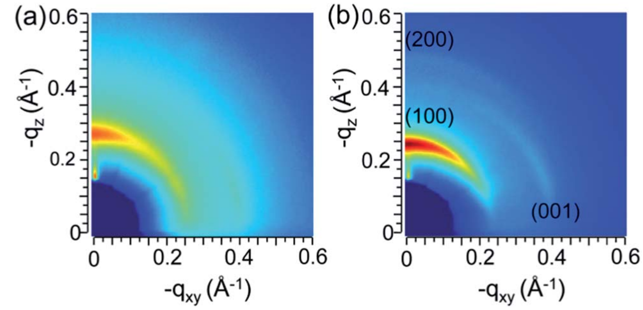

Fig. 3 2D GIXS patterns of **C1** (a) and **C3** (b) thin films.

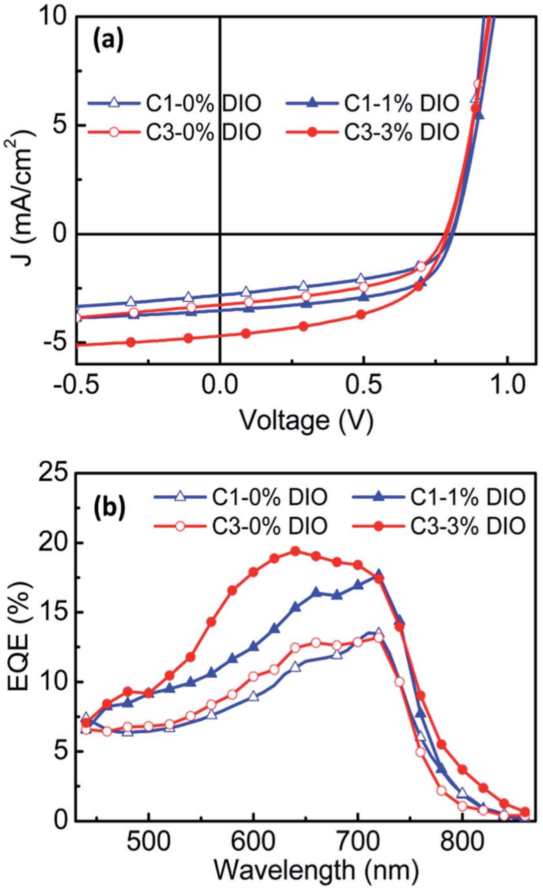

Fig. 4 The current density (*J*)–voltage (*V*) curves (a) and the typical EQE curves (b) of the devices under different conditions.

of the very close V_{oc} and FF, improvement of the efficiency is mainly from the enhanced J_{sc} and high electron mobility, which is probably linked to the optimized morphology of the blend film (*vide infra*).

Moreover, improvement of J_{sc} is supported by the external quantum efficiency (EQE) responses (Fig. 4b), in which the addition of DIO yields an increase of the EQE response. As for the PBDTTT-C-T/**C1** device, 1% DIO addition greatly improved the maximum monochromic EQE from 13.4% to 18.0 % at 720 nm. After further manipulating the alkyl-chain branching position, the maximum value reached 19.6% at 640 nm under the optimal condition, consistent with the highest J_{sc}.

Morphology characterization

TEM and AFM were used to study the phase separation in blend films (processed with DCB or DCB : DIO solvent). TEM images of the blend films are shown in Fig. 5, and the corresponding AFM images are provided in Fig. S3.† In TEM images, the dark regions could be attributed to the acceptor (**C1** or **C3**) domains, while the bright regions could be attributed to the donor (PBDTTT-C-T) domains (depicted in Fig. S4†). When no DIO is added, blend films based on **C1** and **C3** show both dark aggregation domains and small phase separation, which indicates that the poor performances for polymers **C1** and **C3** are related to the non-optimized morphologies. The PBDTTT-C-T/**C3** blend film exhibits more and bigger aggregation domains (*ca.* 15 nm) than the PBDTTT-C-T/**C1** blend film. The

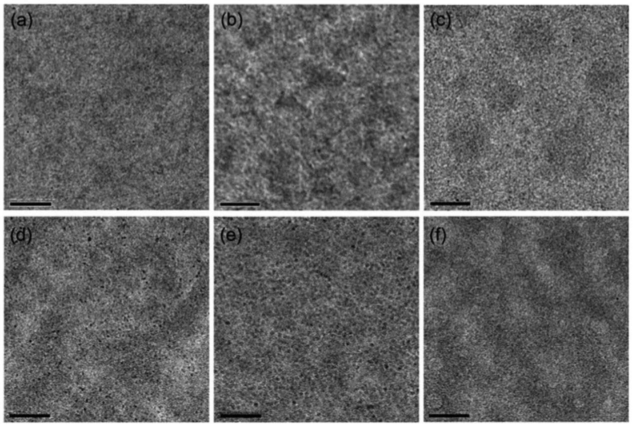

Fig. 5 TEM images of blend films: PBDTTT-C-T:**C1** with (a) 0% DIO, (b) 1% DIO and (c) 2% DIO; PBDTTT-C-T:**C3** with (d) 0% DIO, (e) 3% DIO and (f) 4% DIO. The scale bars are 200 nm.

Table 2 Photovoltaic performances of all-PSC devices based on the two polymers with DCB as solvent and DIO as processing additive

Cn[a]	Solvent (DCB : DIO)[b]	J_{sc}[c] (mA cm^{-2})	V_{oc}[c] (V)	FF[c] (%)	PCE[c] (%) (best[d])
C1	100 : 0	2.88 ± 0.13	0.81 ± 0.01	47.63 ± 1.65	1.11 ± 0.08 (1.21)
	99 : 1	3.56 ± 0.04	0.81 ± 0.00	55.04 ± 1.91	1.59 ± 0.06 (1.68)
C3	100 : 0	3.17 ± 0.09	0.78 ± 0.01	50.65 ± 0.60	1.24 ± 0.03 (1.27)
	97 : 3	4.75 ± 0.11	0.79 ± 0.01	49.29 ± 1.33	1.85 ± 0.05 (1.92)

[a] Cn : donor = 1 : 1 (w/w). [b] DCB : DIO (v/v). [c] Only the optimized recipes were considered for the estimation of the average PCE; data have been averaged for different devices (see ESI). [d] The performance of the best device is given in parentheses. The active area of the device was 0.06 cm^2.

aggregation domains may originate from the better crystallinity, while polymer PBDTTT-C-T is non-crystalline.[52,57] The small improvement of PCE for polymers **C1** and **C3** indicates that polymer crystallinity cannot be the sole factor influencing the performance of devices. Other factors, like the phase domain sizes and ordering of polymer aggregation in the BHJ blends, may also be important because the exciton separation and charge mobility should be efficient across the entire active layer. It is well known that addition of the small-molecule additive DIO into the solvent would optimize the blend morphology in BHJ polymer solar cells.[56,58–60] After 1% DIO is added, PBDTTT-C-T/**C1** blend film exhibits a continuous interpenetrating network with nanoscale phase segregation. Simultaneously, PBDTTT-C-T/**C3** blend film exhibits clear nanoscale phase separation and many dark spots (*ca.* 20 nm in size), which relates to the solubility and crystallization of polymer **C3**. In all-polymer systems, the polymer crystallinity would be an important driving force to form the acceptor domains in this work. The slow rate of evaporation of DIO provides sufficient time for polymer **C3** to aggregate gradually and form a nanoscale phase separation.[56,61] The nanoscale phase separation provides large donor/acceptor interfaces and efficient channels for charge transport, thus leading to high J_{sc} and charge mobility, especially electron mobility. Moreover, the observation in TEM images can also be confirmed by AFM measurements (see Fig. S3†). These results demonstrate that the alkyl-chain branching position significantly influences the nanoscale morphology of blend films by improving polymer crystallinity. A polymer with superior crystallinity could easily aggregate in blends, thus forming a nanoscale morphology.

GIXS was used to provide the structural ordering of the two polymers in blend films (processed with DCB or DCB:DIO mixed solvent) as shown in Fig. 6. The PBDTTT-C-T:**C1** blend film shows ambiguous diffraction arcs; however, the PBDTTT-C-T:**C3** blend film shows much clearer diffraction arcs. This indicates that polymer **C3** in the BHJ blend is more highly ordered than polymer **C1**, which well matches with the crystallinity of the two polymers. The thin films processed from DCB and DCB : DIO mixed solvent yield similar results, which suggests that DIO is beneficial to the aggregation of the two polymers. When the film is cast from DCB : DIO (97 : 3, v/v), several arcs appeared in Fig. 6d, demonstrating that polymer **C3** distributes with highly ordered structure in the BHJ blend film, which enhances the electron transport ability. The clear diffraction arcs in Fig. 6d also provide additional evidence for the clear nanoscale phase separation and aggregation of acceptor **C3**. Consequently, moving the branching position further from the main chain could promote the performance of devices by realizing a nanoscale morphology and highly ordered structure of the polymer.

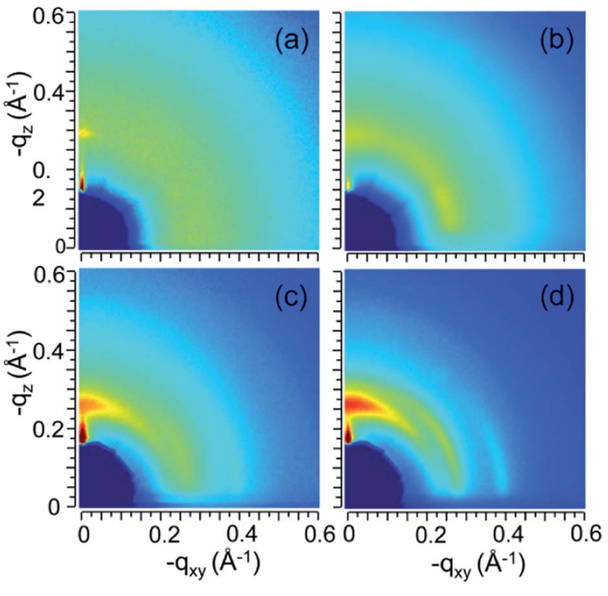

Fig. 6 2D GIXS patterns of blend films: donor:**C1** with 0% DIO (a) and 1% DIO (b); donor:**C3** with 0% DIO (c) and 3% DIO (d).

Conclusions

In conclusion, two polymers based on NDI with different alkyl-chain branching positions, **C1** and **C3**, were synthesized and characterized. It was proved out that the location of the branching point had a significant effect on optical absorption, conjugated backbone orientation, crystallinity, device morphology and charge mobility. Moving the branching position away from the backbone resulted in superior crystallinity of **C3**. From **C1** to **C3**, the morphology in an optimal device showed improved nanoscale morphology and high ordering structure of the polymer. Hence, all-PSCs based on **C3** showed a higher PCE of 1.92%, whereas it was 1.68% for **C1**. Therefore, manipulation of alkyl-chain branching position provides new insights into the design of optimum polymers as acceptors for high performance in all-PSCs.

Acknowledgements

The GIXD data were obtained at 1W1A, Beijing Synchrotron Radiation Facility. The authors gratefully acknowledge the assistance of scientists of the Diffuse X-ray Scattering Station during the experiments. This work was supported by the National Natural Science Foundation of China (no. 20925309, 21190034, 21221002, 21203212) and the National Research Fund for Fundamental Key Project 973 (2011CB808402, 2013CB933500).

Notes and references

1 Y. Zhou, T. Kurosawa, W. Ma, Y. Guo, L. Fang, K. Vandewal, Y. Diao, C. Wang, Q. Yan, J. Reinspach, J. Mei, A. L. Appleton, G. I. Koleilat, Y. Gao, S. C. B. Mannsfeld, A. Salleo, H. Ade, D. Zhao and Z. Bao, *Adv. Mater.*, 2014, **26**, 3767.
2 T. Earmme, Y.-J. Hwang, N. M. Murari, S. Subramaniyan and S. A. Jenekhe, *J. Am. Chem. Soc.*, 2013, **135**, 14960.
3 G. Dennler, M. C. Scharber and C. J. Brabec, *Adv. Mater.*, 2009, **21**, 1323.

4 M. Schubert, D. Dolfen, J. Frisch, S. Roland, R. Steyrleuthner, B. Stiller, Z. Chen, U. Scherf, N. Koch, A. Facchetti and D. Neher, *Adv. Energy Mater.*, 2012, **2**, 369.

5 B. C. Thompson and J. M. J. Fréchet, *Angew. Chem., Int. Ed.*, 2008, **47**, 58.

6 E. Zhou, J. Cong, Q. Wei, K. Tajima, C. Yang and K. Hashimoto, *Angew. Chem., Int. Ed.*, 2011, **50**, 2799.

7 W. Yu, D. Yang, X. Zhu, X. Wang, G. Tu, D. Fan, J. Zhang and C. Li, *ACS Appl. Mater. Interfaces*, 2014, **6**, 2350.

8 D. Mori, H. Benten, I. Okada, H. Ohkita and S. Ito, *Energy Environ. Sci.*, 2014, **7**, 2939.

9 Y. Zhou, T. Kurosawa, W. Ma, Y. Guo, L. Fang, K. Vandewal, Y. Diao, C. Wang, Q. Yan, J. Reinspach, J. Mei, A. L. Appleton, G. I. Koleilat, Y. Gao, S. C. B. Mannsfeld, A. Salleo, H. Ade, D. Zhao and Z. Bao, *Adv. Mater.*, 2014, **26**, 3767.

10 D. Mori, H. Benten, J. Kosaka, H. Ohkita, S. Ito and K. Miyake, *ACS Appl. Mater. Interfaces*, 2011, **3**, 2924.

11 E. Zhou, J. Cong, K. Hashimoto and K. Tajima, *Adv. Mater.*, 2013, **25**, 6991.

12 A. C. Arias, J. D. MacKenzie, R. Stevenson, J. J. M. Halls, M. Inbasekaran, E. P. Woo, D. Richards and R. H. Friend, *Macromolecules*, 2001, **34**, 6005.

13 C. R. McNeill, A. Abrusci, I. Hwang, M. A. Ruderer, P. Müller-Buschbaum and N. C. Greenham, *Adv. Funct. Mater.*, 2009, **19**, 3103.

14 C. R. McNeill and N. C. Greenham, *Adv. Mater.*, 2009, **21**, 3840.

15 M. M. Wienk, J. M. Kroon, W. J. H. Verhees, J. Knol, J. C. Hummelen, P. A. van Hal and R. A. J. Janssen, *Angew. Chem., Int. Ed.*, 2003, **42**, 3371.

16 A. C. Arias, N. Corcoran, M. Banach, R. H. Friend, J. D. MacKenzie and W. T. S. Huck, *Appl. Phys. Lett.*, 2002, **80**, 1695.

17 H. N. Tsao, D. M. Cho, I. Park, M. R. Hansen, A. Mavrinskiy, D. Y. Yoon, R. Graf, W. Pisula, H. W. Spiess and K. Müllen, *J. Am. Chem. Soc.*, 2011, **133**, 2605.

18 J. Mei and Z. Bao, *Chem. Mater.*, 2013, **26**, 604.

19 P. M. Beaujuge and J. M. J. Fréchet, *J. Am. Chem. Soc.*, 2011, **133**, 20009.

20 J. Mei, D. H. Kim, A. L. Ayzner, M. F. Toney and Z. Bao, *J. Am. Chem. Soc.*, 2011, **133**, 20130.

21 H. Sirringhaus, P. J. Brown, R. H. Friend, M. M. Nielsen, K. Bechgaard, B. M. W. Langeveld-Voss, A. J. H. Spiering, R. A. J. Janssen, E. W. Meijer, P. Herwig and D. M. de Leeuw, *Nature*, 1999, **401**, 685.

22 I. McCulloch, M. Heeney, C. Bailey, K. Genevicius, I. MacDonald, M. Shkunov, D. Sparrowe, S. Tierney, R. Wagner, W. Zhang, M. L. Chabinyc, R. J. Kline, M. D. McGehee and M. F. Toney, *Nat. Mater.*, 2006, **5**, 328.

23 B. S. Ong, Y. Wu, P. Liu and S. Gardner, *J. Am. Chem. Soc.*, 2004, **126**, 3378.

24 F. Zhang, Y. Hu, T. Schuettfort, C. Di, X. Gao, C. R. McNeill, L. Thomsen, S. C. B. Mannsfeld, W. Yuan, H. Sirringhaus and D. Zhu, *J. Am. Chem. Soc.*, 2013, **135**, 2338.

25 M. S. Chen, J. R. Niskala, D. A. Unruh, C. K. Chu, O. P. Lee and J. M. J. Fréchet, *Chem. Mater.*, 2013, **25**, 4088.

26 A. C. Mayer, M. F. Toney, S. R. Scully, J. Rivnay, C. J. Brabec, M. Scharber, M. Koppe, M. Heeney, I. McCulloch and M. D. McGehee, *Adv. Funct. Mater.*, 2009, **19**, 1173.

27 N. Wang, Z. Chen, W. Wei and Z. Jiang, *J. Am. Chem. Soc.*, 2013, **135**, 17060.

28 I. Osaka, M. Saito, T. Koganezawa and K. Takimiya, *Adv. Mater.*, 2014, **26**, 331.

29 I. Meager, R. S. Ashraf, S. Mollinger, B. C. Schroeder, H. Bronstein, D. Beatrup, M. S. Vezie, T. Kirchartz, A. Salleo, J. Nelson and I. McCulloch, *J. Am. Chem. Soc.*, 2013, **135**, 11537.

30 C. Piliego, T. W. Holcombe, J. D. Douglas, C. H. Woo, P. M. Beaujuge and J. M. J. Fréchet, *J. Am. Chem. Soc.*, 2010, **132**, 7595.

31 Y. Liang and L. Yu, *Acc. Chem. Res.*, 2010, **43**, 1227.

32 J. Warnan, C. Cabanetos, R. Bude, A. El Labban, L. Li and P. M. Beaujuge, *Chem. Mater.*, 2014, **26**, 2829.

33 C. Cabanetos, A. El Labban, J. A. Bartelt, J. D. Douglas, W. R. Mateker, J. M. J. Fréchet, M. D. McGehee and P. M. Beaujuge, *J. Am. Chem. Soc.*, 2013, **135**, 4656.

34 S. Subramaniyan, H. Xin, F. S. Kim, S. Shoaee, J. R. Durrant and S. A. Jenekhe, *Adv. Energy Mater.*, 2011, **1**, 854.

35 T. W. H. Claudia Piliego, J. D. Douglas, C. H. Woo, P. M. Beaujuge and J. M. J. Frèchet, *J. Am. Chem. Soc.*, 2010, **132**, 3.

36 X. Guo and M. D. Watson, *Org. Lett.*, 2008, **10**, 5333.

37 C. Gu, W. Hu, J. Yao and H. Fu, *Chem. Mater.*, 2013, **25**, 2178.

38 H. Chen, Y. Guo, Z. Mao, G. Yu, J. Huang, Y. Zhao and Y. Liu, *Chem. Mater.*, 2013, **25**, 3589.

39 K. Tremel, F. S. U. Fischer, N. Kayunkid, R. D. Pietro, R. Tkachov, A. Kiriy, D. Neher, S. Ludwigs and M. Brinkmann, *Adv. Energy Mater.*, 2014, **4**, 1301659.

40 Y. Kim, J. Hong, J. H. Oh and C. Yang, *Chem. Mater.*, 2013, **25**, 3251.

41 R. Steyrleuthner, R. Di Pietro, B. A. Collins, F. Polzer, S. Himmelberger, M. Schubert, Z. Chen, S. Zhang, A. Salleo, H. Ade, A. Facchetti and D. Neher, *J. Am. Chem. Soc.*, 2014, **136**, 4245.

42 A. Luzio, D. Fazzi, D. Natali, E. Giussani, K.-J. Baeg, Z. Chen, Y.-Y. Noh, A. Facchetti and M. Caironi, *Adv. Funct. Mater.*, 2014, **24**, 1151.

43 S. Fabiano, Z. Chen, S. Vahedi, A. Facchetti, B. Pignataro and M. A. Loi, *J. Mater. Chem.*, 2011, **21**, 5891.

44 Y.-J. Hwang, G. Ren, N. M. Murari and S. A. Jenekhe, *Macromolecules*, 2012, **45**, 9056.

45 Z.-K. Tan, K. Johnson, Y. Vaynzof, A. A. Bakulin, L.-L. Chua, P. K. H. Ho and R. H. Friend, *Adv. Mater.*, 2013, **25**, 4131.

46 T. W. Holcombe, J. E. Norton, J. Rivnay, C. H. Woo, L. Goris, C. Piliego, G. Griffini, A. Sellinger, J.-L. Brédas, A. Salleo and J. M. J. Fréchet, *J. Am. Chem. Soc.*, 2011, **133**, 12106.

47 J. R. Moore, S. Albert-Seifried, A. Rao, S. Massip, B. Watts, D. J. Morgan, R. H. Friend, C. R. McNeill and H. Sirringhaus, *Adv. Energy Mater.*, 2011, **1**, 230.

48 P. Liu, K. Zhang, F. Liu, Y. Jin, S. Liu, T. P. Russell, H.-L. Yip, F. Huang and Y. Cao, *Chem. Mater.*, 2014, **26**, 3009.

49 W. Li, L. Yang, J. R. Tumbleston, L. Yan, H. Ade and W. You, *Adv. Mater.*, 2014, **26**, 4456.

50 X. Xu, Y. Wu, J. Fang, Z. Li, Z. Wang, Y. Li and Q. Peng, *Chem. Eur. J.*, 2014, 1.

51 K. G. Jespersen, W. J. D. Beenken, Y. Zaushitsyn, A. Yartsev, M. Andersson, T. Pullerits and V. Sundström, *J. Chem. Phys.*, 2004, **121**, 12613.

52 L. Huo, S. Zhang, X. Guo, F. Xu, Y. Li and J. Hou, *Angew. Chem.*, 2011, **123**, 9871.

53 Y. Li, S. P. Singh and P. Sonar, *Adv. Mater.*, 2010, **22**, 4862.

54 J. Peet, J. Y. Kim, N. E. Coates, W. L. Ma, D. Moses, A. J. Heeger and G. C. Bazan, *Nat. Mater.*, 2007, **6**, 497.

55 M. Han, H. Kim, H. Seo, B. Ma and J.-W. Park, *Adv. Mater.*, 2012, **24**, 6311.

56 J. K. Lee, W. L. Ma, C. J. Brabec, J. Yuen, J. S. Moon, J. Y. Kim, K. Lee, G. C. Bazan and A. J. Heeger, *J. Am. Chem. Soc.*, 2008, **130**, 3619.

57 L. Huo, L. Ye, Y. Wu, Z. Li, X. Guo, M. Zhang, S. Zhang and J. Hou, *Macromolecules*, 2012, **45**, 6923.

58 J. J. Jasieniak, B. B. Y. Hsu, C. J. Takacs, G. C. Welch, G. C. Bazan, D. Moses and A. J. Heeger, *ACS Nano*, 2012, **6**, 8735.

59 L. Gang, Z. Rui and Y. Yang, *Nat. Photonics*, 2012, **6**, 153.

60 J. Peet, M. L. Senatore, A. J. Heeger and G. C. Bazan, *Adv. Mater.*, 2009, **21**, 1521.

61 J. Huang, C. Zhan, X. Zhang, Y. Zhao, Z. Lu, H. Jia, B. Jiang, J. Ye, S. Zhang, A. Tang, Y. Liu, Q. Pei and J. Yao, *ACS Appl. Mater. Interfaces*, 2013, **5**, 2033.